Research Highlights

The past year saw over 100 papers published or accepted for publication in peer-reviewed journals, across all of the Centre's ten experimental and nine theoretical research programs. The next few pages bring together the key research highlights for 2009 across the Centre.

Silicon-based Si:P Qubits: Top-Down Fabrication and Measurement

The development of spin-based qubits in the Si:P material system is the key focus of the Centre's solid-state programs. At UNSW the Integrated Quantum Computer Devices program and the Quantum Measurement program interact closely with the University of Melbourne's Ion Beam and Device Modelling programs to design, construct and measure silicon-based qubits and qubit test devices.

During 2009 the teams published a new spin-qubit design that is entirely compatible with MOS processes and which offers high-fidelity spin readout [Morello *et al*., **Physical Review B 80**, 081307 (2009)].

The architecture combines:

(i) accurate P donor implantation via our existing single-ion counting technology
(ii) new capabilities developed at UNSW for local electron spin resonance of phosphorus donors [Willems van Beveren *et al*., **Applied Physics Letters 93**, 07102 (2008)] which enables coherent spin manipulation; and
(iii) an integrated silicon single electron transistor (Si-SET) which we have developed, that can be used for spin-to-charge conversion readout in DC mode [Angus *et al*., **Nano Letters 7**, 2051 (2007)] or RF mode [Angus *et al*., **Applied Physics Letters 92**, 112103 (2008)].

In 2009 we have used such an architecture to demonstrate, for the first time, the *single-shot readout of a single electron spin in silicon*, with a high readout fidelity above 90% [Morello *et al*., **arXiv:1003.2679** – submitted to Nature]. This landmark result represents a crucial step in the demonstration of spin-based quantum computing in silicon.

The device used for the experiments is shown in Figure 1, along with the gate biasing and pulsing circuitry. A dc bias is applied to the Si-SET and the current is measured using a high-bandwidth (up to 200 kHz) preamplifier. Voltage pulses are then applied to the gate above the implanted P donors to carry out the spin readout protocol.

A single-shot spin readout sequence consists of a 3-level pulse that shifts the electrochemical potential of the donor electron with respect to the SET island (Figure 2). In the "load" phase, an electron with random spin is loaded onto the donor. In the "read" phase, the spin-up and spin-down states are tuned above and below the electrochemical potential of the SET island, respectively.

Therefore, when a spin-up electron is present, it first tunnels off the donor, unblocking the SET current, until a spin-down electron tunnels on again. This results in a characteristic "blip" of current that can be easily resolved. Finally, the "empty" pulse flushes the electron away from the donor, to make sure that a new electron with random spin can be loaded in the next cycle.

Figure 2 shows the method to determine the correct read level for spin readout. The SET current as a function of the "read" pulse voltage goes from high, to showing random telegraph noise, through the correct value where either no blip (spin-down) or one single blip (spin-up) is observed.

By varying the time τ the electron spends on the donor during the "load" pulse, we have measured the spin relaxation rate $1/T_1$ (Figure 3). The results are in qualitative and quantitative agreement with theoretical predictions and bulk spin-resonance experiments of P donors in silicon. The magnetic field dependence is described by $1/T_1(B) = K_0 + K_5 B^5$, where the term $\propto B^5$ is characteristic of relaxation via spin-orbit coupling, while the constant term may be due to dipolar flip-flops with nearby donors. The longest relaxation time we have observed is $T_1 \approx 0.9$ s at $B = 1.75$ T.

Due to the high charge transfer signal, i.e. the large change in SET current when an electron tunnels on or off the donor, we achieve a very high readout visibility $> 90\%$ with a detection bandwidth ~100 kHz, corresponding to a readout time < 10 μs.

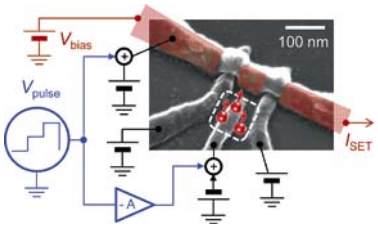

FIGURE 1

Circuit diagram and SEM image of the qubit device employed for single-shot spin readout.

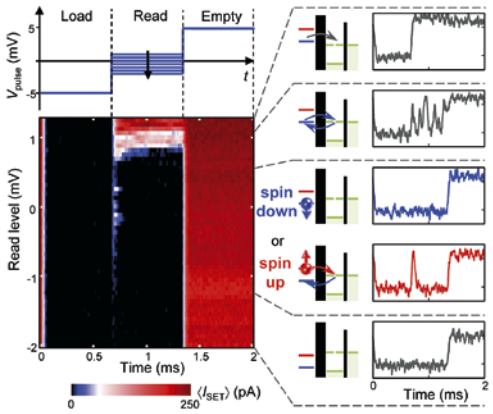

FIGURE 2

Three-level pulse sequence for single-shot spin readout. The main panel shows averaged SET current as a function of the "read" pulse voltage. The time-resolved single-shot traces highlight the correct tuning region where projective readout of spin-down (blue) or spin-up (red) electrons is obtained.

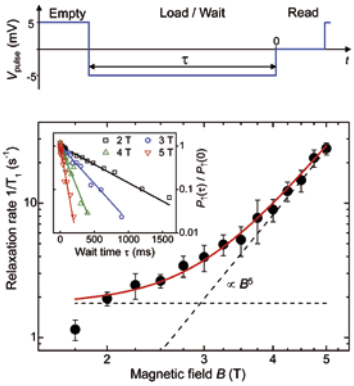

FIGURE 3

Field dependence of the spin lattice relaxation rate ($1/T_1$), obtained by varying the wait time τ in the 3-level pulse sequence. Inset: exponential decays of the spin-up fraction $P\uparrow$ at different magnetic fields.

Atomic Precision Qubits

Over the past year the Atomic Fabrication and Crystal Growth Program has made tremendous progress in the miniaturisation of single crystal phosphorus doped silicon quantum dots. The aim of the program has been to reduce the number of P atoms in the dots towards the single donor level using an approach based on all epitaxial highly phosphorus doped silicon in-plane gates (A. Fuhrer *et al*., **Nano Letters** 9, 707 (2009)) so that we can control electron transport through the donor and measure its excitation spectrum. The advantage of an all epitaxial approach is that ultimately we will have P atom qubits that are far removed from surface and interface states and are surrounded by a crystalline environment. Such an environment is expected to allow spin qubits to maintain their coherence for longer times and, when combined with atomically precise dopant placement, should allow scalable qubit architectures.

Figure 4 shows the lithography of a few donor dot fabricated using STM lithography. We can see the sub nm precision patterning of the central dot region, which after phosphine dosing and incorporation contains ~7 P atoms. The stability plot in Figure 5 shows the colour-scale plot of the differential conductance d*I*/dV_{SD} through the quantum dot. Here we see 7 Coulomb diamonds and a series of striking white lines running parallel to both diamond edges. These are the excited state lines due to transport through the dot.

The height of each dark diamond is the addition energy, which changes from 25 meV to 45 meV—the latter value being close to the limit of a single phosphorus donor in silicon—as five electrons are removed from the dot. Such a dramatic change in energy is only possible when the quantum dot is in the few-electron limit, so the removal of five electrons causes the size of the dot to change significantly.

Figure 6 shows a high-resolution scan of one of the transitions. The data reveal a dense set of excited-state resonances, with an average spacing of 100 μeV. The appearance of this dense, closely spaced set of conduction resonances is a surprising feature of such a small quantum dot. This separation is too small to be explained by the nanometre-scale size of the device. We have worked with Professor Mark Eriksson and Dr Mark Friesen at the University of Wisconsin-Madison to model what can give rise to this dense excitation spectrum. Using effective mass modeling we were able to show that the abrupt lateral confinement potential of the dot lifted the degeneracy of the Δ-valleys in the conduction band giving rise to the dense set of many-body excited states observed. Additionally, the narrow confinement in the source and drain regions was shown to give singularities in the density of states with ~10 meV separation. The combination of these two effects provides a consistent explanation for the complete resonance spectrum observed.

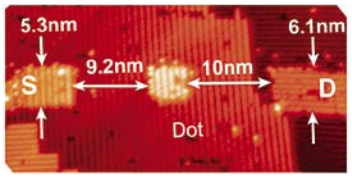

FIGURE 4:
STM lithography showing a 4.6×4.6nm desorbed area which will incorporate 7 P donors.

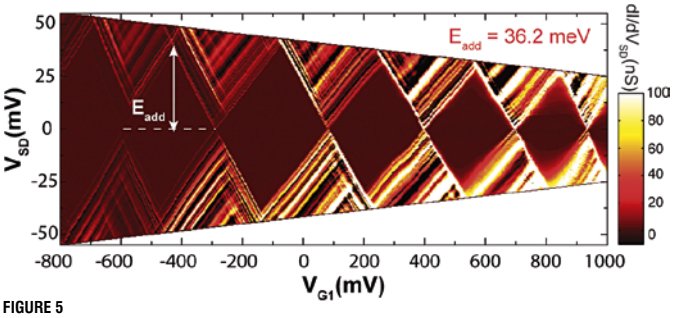

FIGURE 5
The stability diagram for a 7 donor dot showing a dense spectrum of excited states.

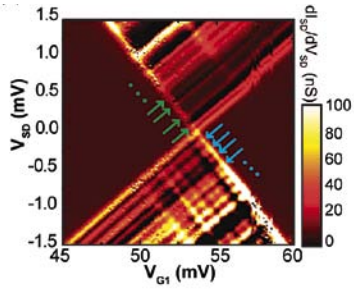

FIGURE 6
A close-up of one of the Coulomb blockade transitions for a 7 donor dot showing a dense spectrum of excited states.

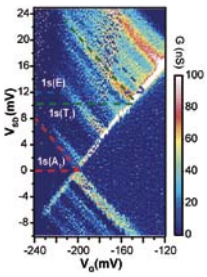

FIGURE 7:
The stability diagram for a single donor dot showing an addition energy of 42±2meV and lines at the excited state energies of 11 and 13 meV. Additional lines observed are due to the one dimensional subbands of the lead geometry.

Following this we fabricated a single donor device. If the dense set of resonances with ~100μeV separation are due to the splitting of the electrons in the Δ-bands, then by dropping the donor number we should depopulate these bands and only observe an energy level splitting due to the occupation of the Γ-bands. This would give rise to a much higher ~meV splitting. This is indeed what we observed, see Figure 7. The stability plot in Figure 7 shows the presence of a single diamond with a charging energy of 42±2meV, consistent with a bulk donor in silicon. Furthermore we no longer see 100μeV splitting but see lines at ~11 and 13meV which correspond to the excited 1s(T_1) and 1s(E) states of a single donor. Additional lines in the spectrum are also observed at ~5meV and have been calculated to be due to the additional one-dimensional subbands of the lead geometry. An exciting development over the past year has been this increased interaction with theoretical groups. This also includes intensive work undertaken with the modelling groups of Prof Klimeck (Purdue) and Prof Hollenberg (Melbourne) to understand the nature of transport in the 1D leads and to understand the definitive signatures of a single donor device.

Over the past year a key highlight has therefore been that we have reduced the donor number to the single donor limit – an extremely important and exciting result. Work is currently underway to perform EDMR measurements of these devices to show the ability to manipulate the spin states of the donor.

Optical Qubits: Experiment and Theory

The optical quantum computing teams at the University of Queensland, Griffith University and the University of New South Wales @ the Australian Defence Force Academy continue to perform world class research at the cutting edge of this discipline. In the following we discuss some highlights.

QUANTUM PARAMETER ESTIMATION

Quantum parameter estimation (QPE) is the problem of estimating an unknown classical parameter or process of a quantum system. It plays a key role in the preparation or dynamics of quantum systems. QPE has many applications, from gravitational wave detection to quantum computing. This year we achieved the first experimental demonstration of QPE using quantum smoothing and continuous adaptive phase techniques. Using these techniques we were able to demonstrate an improvement of more than a factor of 2 over the standard quantum limit (see Figure 8). This work was a major international collaboration led by A/Prof Elanor Huntington's group at UNSW@ADFA and involving the group of Prof Akira Furusawa at the University of Tokyo, researchers at the Perimeter institute and University of Waterloo in Canada, as well as Centre researchers Prof Howard Wiseman (Griffith) and Prof Tim Ralph (UQ). This research has appeared as T.A. Wheatley *et al*, **Physical Review Letters 104**, 093601 (2010).

HERALDED NOISELESS LINEAR AMPLIFICATION AND DISTILLATION OF ENTANGLEMENT

A ubiquitous process in classical computing and communications is amplification. Quantum mechanics places fundamental limits on amplification that lead to the inevitable coupling of noise onto the amplified signal. A loophole that allows noiseless amplification of quantum systems is to introduce a probabilistic amplifier that only works some of the time but tells you when it does. Such a device would find many applications in quantum information protocols. This year we have proposed and demonstrated such a noiseless amplifier for optical modes (see Figure 9) and used it to distill field entanglement. Entanglement distillation can be used to extend the length of quantum communication protocols or as an error correction technique in quantum computing. This research was led by A/Prof Geoff Pryde's group from Griffith University using the protocol developed by Prof Tim Ralph's group at UQ and has appeared as G.Y. Xiang *et al.*, **Nature Photonics 4**, 316 (2010).

QUANTUM COMPUTING USING HIGHER-DIMENSIONS

Most approaches to quantum computing use qubits, a two-level quantum system. Realizing qubits typically requires enforcing a two-level structure on systems that are naturally far more complex and which have many readily accessible degrees of freedom, such as atoms, ions or photons. It has been shown by Prof Tim Ralph's group at UQ that harnessing these extra levels during computation significantly reduces the number of elemental gates required to build key quantum circuits. Because the technique is independent of the physical encoding of quantum information and the way in which the elemental gates are themselves constructed, it has the potential to be used in conjunction with existing gate technology in a wide variety of architectures. An experimental demonstration of these techniques, led by Prof Andrew White's group at UQ and in collaboration with A/Prof Geoff Pryde's group at Griffith and researchers at Bristol and Waterloo Universities, has appeared as B.Lanyon *et al* **Nature Physics 5**, 134 (2009). Prof White's group, with collaborators from Harvard University in the US, have subsequently used these techniques to demonstrate key steps in the simulation of quantum chemistry on a quantum computer. This work has appeared as B. Lanyon *et al.*, **Nature Chemistry 2**, 106 (2010).

STEERING ENTANGLEMENT

The understanding of entanglement is key to many quantum information protocols. The group of Prof Howard Wiseman at Griffith have continued to investigate the concept of steering entanglement, introduced by Schrödinger as a generalization of the Einstein-Podolsky-Rosen (EPR) paradox but only recently formalized by the Griffith group with a collaborator at UQ. In 2009 a general theory of experimental EPR-steering criteria was developed and a number of criteria applicable to discrete as well as continuous variable observables were derived. This work has appeared as Cavalcanti *et al.*, **Phys. Rev. A 80**, 032112 (2009). An experimental demonstration of these techniques has been performed by the group of A/Prof Geoff Pryde at Griffith that is described in D. J. Saunders, *et al* arXiv:0909.0805 (2009).

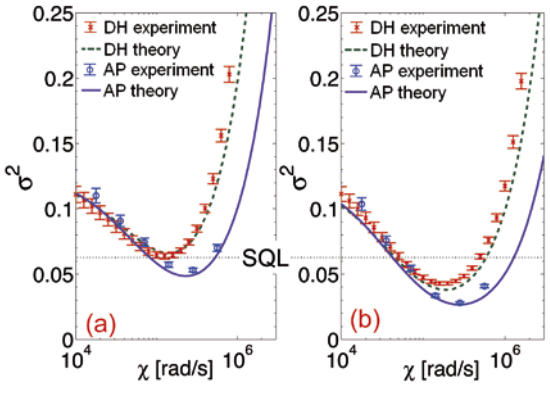

FIGURE 8

The experimental and theoretical variance of the four phase estimation techniques: filtered dual homodyne (DH) and adaptive phase (AP) in part (a); and smoothed DH and AP in part (b).

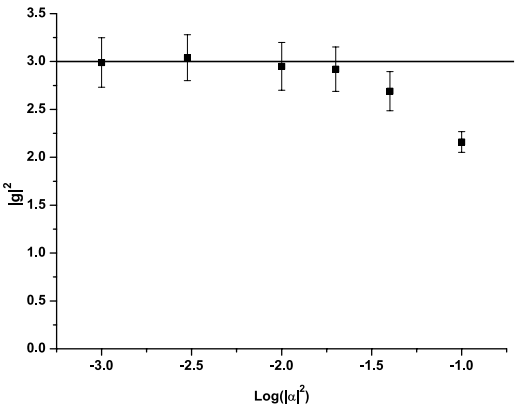

FIGURE 9

Gain of the noiseless amplifier as a function of input state size, showing linear behaviour until saturation.

Quantum Computing Theory

In 2009 we produced a number of significant results in diverse areas from quantum computing to quantum communication and decoherence sensing. Here we list some highlights.

MAPPING THE DONOR WAVE FUNCTION USING SI(29) SPINS

Control of the donor electron wave function is central to any quantum information technology based on donors in silicon. In the paper S. H. Park *et al*, *Mapping Donor Electron Wave Function Deformations at a Sub-Bohr Orbit Resolution*, **Physical Review Letters 103** 106802 (2009) by Purdue student Seung Park in collaboration with CQCT/SNL researchers we proposed an electron-nuclear double resonance experiment to directly measure the gate induced Stark shift of the donor electron hyperfine tensor at specific lattice sites near the donor site. Si(29) atoms naturally and randomly distributed in the lattice provide a direct nuclear spin probe of the donor electron wave function within the Bohr orbit region. Our atomistic tight-binding simulations for multi million atom devices, show that this technique could provide a spatial map of the response of the donor electron wave function to a controlling gate field to sub-Bohr orbit resolution.

SURFACE CODE BASED QUANTUM COMMUNICATION PROTOCOL

An ideal quantum communication protocol should permit the rapid transmission of data while simultaneously tolerating a high rate of loss of photons and a high rate of error on transmitted photons, and employ quantum repeater resources efficiently. In the paper A. Fowler *et al*, *Surface code quantum communication*, **Physical Review Letters** in press, we have adapted the powerful surface error correction code for quantum communication. In principle up to 50% of the photons can be lost and the remaining photons can effectively have an error rate of almost 100%. In simulations, we have found that when both loss and error are considered, 35% loss and 5% error can be tolerated efficiently. This means that data can be transmitted at MHz rates and the addition of a few hundred qubits into each repeater enables the transmission distance to be increased by an order of magnitude with no additional error.

QUANTUM DECOHERENCE SENSING USING SPINS IN DIAMOND

The use of qubits as sensitive nano-scale probes is of great interest as a near-term quantum technology application. Program researchers have proposed decoherence measurements as a sensitive measure of magnetic field fluctuations. In the paper L. Hall *et al*, *Sensing of Fluctuating Nanoscale Magnetic Fields Using Nitrogen-Vacancy Centers in Diamond*, **Physical Review Letters 103** 220802 (2009) by PhD student Liam Hall and UM CQCT researchers we showed that the nitrogen-vacancy (NV) centre in diamond is an ideal qubit system for room temperature biological applications of decoherence sensing. In a follow-up paper L. Hall, *Monitoring Ion Channel Function In Real Time Through Quantum Decoherence*, **arXiv:0911.4539** (2009) we For the first time we explored in detail the quantum dynamics of a NV probe in the extra-cellular environment, proximate to an ion channel. Our results indicate that real-time detection of ion channel operation at millisecond resolution is possible by directly monitoring the quantum decoherence of the NV probe.

THRESHOLD OF THE COLOUR CODE ERROR CORRECTION SCHEME

The colour code is a quantum error correcting code of interest as its physical implementation requires only a 2-D array of qubits with nearest neighbour interactions, and permits a wide range of logical gates to be applied directly to protected data in a transversal manner. The classical processing required to determine the maximum permitted error rates of the various components in such a quantum computer had never been attempted until the work of PhD student David Wang in D. Wang *et al*, *Graphical algorithms and threshold error rates for the 2d colour code*, **arXiv:0907.1708** (2009). We considered two error scenarios – errors on data qubits only and errors on all qubits and after all gates. In the first scenario, we found that the error correction works provided the data qubit error rate is below 13.3%. In the second scenario, we found that the error rates of all components must be below 0.1%.

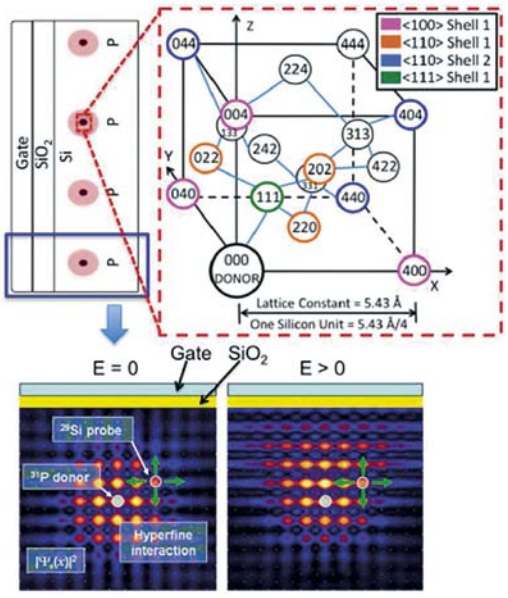

FIGURE 10

Probing and mapping the field-induced distortions of the donor wave function by a Si(29) atoms using hyperfine interaction.

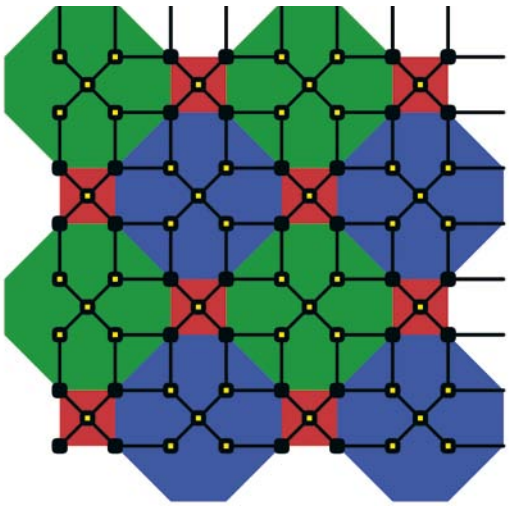

FIGURE 11

Colour code arrangement of data qubits (black dots), syndrome qubits (yellow dots) and nearest neighbour interactions (black lines).